Numerical studies on minimum ignition energies in methane/air and iso-octane/air mixtures[☆]

Chunwei Wu [*], Robert Schießl, Ulrich Maas

Institute of Technical Thermodynamics, Karlsruhe Institute of Technology, Engelbert-Arnold-Str. 4, Karlsruhe, 76131, Germany

ARTICLE INFO

ABSTRACT

In this study, the dependence of minimum ignition energies (MIE) on ignition geometry, ignition source radius and mixture composition is investigated numerically for methane/air and iso-octane/air mixtures. Methane and iso-octane are both important hydrocarbon fuels, but differ strongly with respect to their Lewis numbers. Lean iso-octane air mixtures have particularly large Lewis numbers. The results show that within the flammability limits, the MIE for both mixtures stays almost constant, and increases rapidly at the limits. The MIEs for both fuels are also similar within the flammability limits. Furthermore, the MIEs of iso-octane/air mixtures with a small spherical ignition source increase rapidly for lean mixtures. Here the Lewis number is above unity, and thus, the flame may quench because of flame curvature effects. The observations show a distinct difference between ignition and flame propagation for iso-octane. The minimum energy required for initiating a successful flame propagation can be considerably higher than that required for initiating an ignition in the ignition volume. For iso-octane with a small spherical ignition source, this effect was observed at all equivalence ratios. For iso-octane with cylindrical ignition sources, the phenomenon appeared at lower equivalence ratios only, where the mixture's Lewis number is large. For methane fuel, the effect was negligible. The results highlight the significance of molecular transport properties on the decision whether or not an ignitable mixture can evolve into a propagating flame.

1. Introduction

Flame initiation is one of the essential problems in combustion. It is either desired, e.g., in gasoline engines, or one seeks to prevent it, like in explosion-critical environments. In both cases, understanding details of the flame initiation and early flame propagation can help improving processes. In IC engines, this understanding allows for improved designs with better fuel efficiency and lower emission. Thus, the investigation of flame initiation is important for combustion engines. In safety engineering it is important for avoiding unwanted ignition processes (Chakrabarty et al., 2016; Dahn and Dastidar, 2003; Hansen and Middha, 2008).

It is well known that for a successful induced ignition, a minimum ignition energy (MIE) is needed to achieve high temperatures of the fuel-air mixture in the ignition volume to allow fast chemical reactions to commence (see e.g. Warnatz et al. (2006)). This leads to the formation of a flame kernel, which then might give rise to further propagation of a self-sustained flame. In the past, the dependence of MIE on the pressure,

initial temperature, mixture stoichiometry and ignition source volume for different fuels has been investigated (Frendi and Sibulkin, 1990; Lewis and von Elbe, 1987; Maas and Warnatz, 1988). There are two possibilities after a certain amount of external energy is deposited: the spherical flame propagates outwardly and finally becomes a planar flame or the flame quenches.

The flame initiation and early propagation of the simpler fuels such as hydrogen or methane is well studied. For iso-octane, an important component and model fuel for gasoline, less studies are available. Beside its practical significance, the case of induced ignition in iso-octane/air mixtures is also interesting from a more fundamental viewpoint, because at least two physical or chemical aspects of this fuel are more complicated than for CH_4. First of all, the Lewis number (Renner, 2007)) of iso-octane/air mixtures is very different from that of methane/air mixtures: while the Lewis number for methane/air mixtures is overall close to 1 at atmospheric pressure and room temperature (Clarke, 2002), the Lewis number of iso-octane/air mixtures varies from under unity at rich condition to 3 for lean mixtures (Abdel-Gayed et al., 1985; Takashi

and Kimitoshi, 2006). Also, iso-octane as a higher hydrocarbon features a more complicated chemistry during its oxidation compared to methane; also in this behavior, iso-octane is closer to most practical gasoline-type fuels than methane.

This work aims to investigate the MIEs for methane and iso-octane with different fuel compositions (throughout the flammable range), different ignition source geometries (spherical and cylindrical) and different ignition source sizes (0.5 mm–3 mm) at 1 bar and 298 K, in order to find out the ignition properties of the two fuels, and to better understand how the interplay of chemical reaction and transport effects (in particular, species diffusion and heat conduction) affect the ignition process. It uses numerical simulations, involving a detailed treatment of chemical reactions and molecular transport effects, for this.

2. Numerical method

Model simulations of flame initiation were performed using the in-house code INSFLA (Maas and Warnatz, 1988). This code solves Navier-Stokes equations in implicit time stepping with error control, and computes the temporal evolution of combustion processes in one-dimensional geometries, considering detailed chemistry and detailed molecular transport. Running the code delivers spatiotemporal profiles of temperature and species.

The simulations use a domain which depends on one spatial variable r; this can describe cylindrically symmetric domains with infinite extent in axial direction, and also spherically symmetric domains. Simulations are initialized with a compositionally and thermally homogeneous fuel/air mixture with some predefined initial conditions. The calculations assume constant pressure (1 bar). The initial temperature is 298 K, which is a typical ambient temperature, and is often used in experiments and simulations. Premixed methane/air mixtures and iso-octane/air mixtures were used as fuels in this present study. We used the GRI 3.0 mechanism with 53 species and 325 reactions to describe the detailed chemical kinetics of methane (Smith et al.). A semi-detailed chemical kinetics model for Toluene Reference Fuels (TRF) with 137 species and 633 reactions is used, which also contains chemistry for iso-octane (Andrae et al., 2008). The air used in this study has a composition of 21% O_2 and 79% N_2 by mole. The investigated fuel compositions are varied within an interval that includes the flammability limits (from φ 0.46 to φ 1.86 for methane/air mixtures and from φ 0.77 to φ 4.57 for iso-octane/air mixtures). Zero gradient boundary condition is used for both temperature and species concentration calculations.

Starting from t 0, an energy source term is applied for a duration (ignition duration) of 10^{-4} s in a region (whose size is defined by the ignition radius r_s) at the inner domain boundary (r 0). In the following, this region will be referred to as ignition kernel. We considered both spherical and cylindrical ignition kernels. For each ignition geometry, several ignition radii (ranging from r 0.5 mm to r 3 mm) were investigated.

The strength of the source is characterized by its energy density q, which has an exponential form, see Fig. 1 (Maas and Warnatz, 1988):

$$q \quad q_{max} \times e^{\left(\frac{r}{r_s}\right)^8} \tag{1}$$

For spherical geometry, E is the total energy deposited at the center of the gas mixture, E is in J. The maximum energy density then is (note that the factor is a result of the fact that the source has an exponential shape and is not constant within the source volume) (Maas and Warnatz, 1988)

$$q_{sph} \quad 0.889 \times \frac{E_{sph}}{\frac{4}{3}\pi r_s^3} \tag{2}$$

For cylindrical geometry (infinite cylinder (Maas and Warnatz, 1988),), E is the deposited energy per length of the infinite cylinder, and has a unit of J/m. The energy density then is (Maas and Warnatz, 1988)
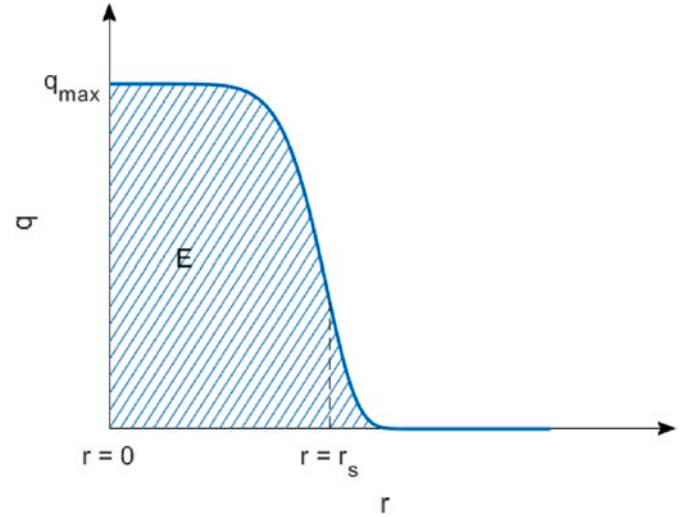

Fig. 1. The exponential form of the ignition energy density.

$$q_{cyl} \quad 0.906 \times \frac{E_{cyl}}{\pi r_s^2} \tag{3}$$

The computational domain size for $r_s \leq 1$ mm was set to 0.01 m, while for $r_s > 1$ mm, it was set to 0.05 m. Thus, there was sufficient space to make sure the outer boundary of the domain did not affect the ignition process and early phase of flame propagation.

One-dimensional simulations are used in this study. Two or three dimensional effects cannot be accounted for. However, in our study, the outer boundary is set to be large enough, so that the outer boundary would not affect the flame initiation and early propagation process. Thus, useful insights of the interaction between chemical reactions and transport processes and how it affects the minimum ignition energy can still be obtained by one-dimensional simulation.

Temperature profiles are analysed to decide between flame propagation and flame extinction. For example, Fig. 2 shows the temperature profiles for the case of a successful ignition (diagram (a)), and also for an ignition failure (diagram (b)). As can be seen, in a successful ignition, the temperature in the center of the mixture rises and a flame kernel is formed; after some time, a self-sustaining flame starts to propagate outwards. On the other hand, in an ignition failure, the heat is conducted to the surroundings, and the temperature at the center finally decreases back to 298 K.

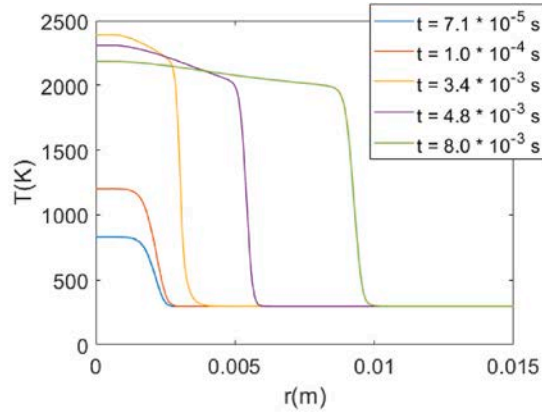## 3. Results and discussion

3.1. Minimum ignition energies for methane/air mixtures and iso-octane/air mixtures

Fig. 3 shows the minimum ignition energies in dependence on the equivalence ratio φ, with a spherical ignition source for methane/air mixtures and iso-octane/air mixtures. In the diagrams, a normalized equivalence ratio is used:

$$\varphi_n \quad \frac{\varphi}{\varphi + 1} \tag{4}$$

This allows showing both the rich ($\varphi > 1$, $\varphi_n > 0.5$) and lean ($\varphi < 1$, $\varphi_n < 0.5$) sides of the flammable range in a nearly symmetric fashion (Law, 2006).

The minimum ignition energies here are to be understood as the minimum energies required for creating a stable flame. Above the MIE, the system evolves into a self-sustained, propagating flame. Below the MIE, two patterns of evolution can be observed: Either the mixture in the ignition volume is not ignited at all, or a flame kernel is formed, but the
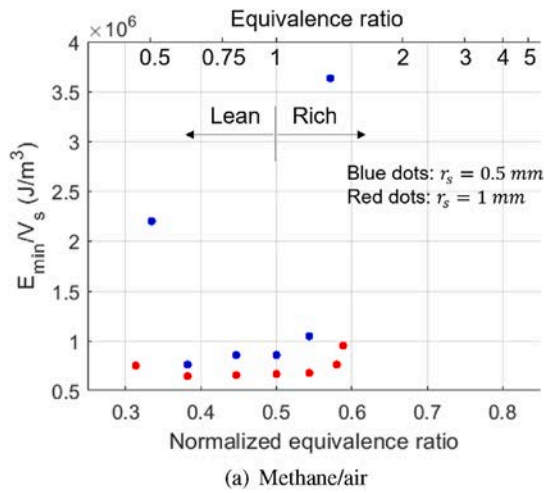
(a) The temperature history for the case of a successful ignition. (iso-octane/air mixture, $\phi = 1.60$, spherical geometry, $r_s = 2\,mm$, $q = 5.13 \times 10^5\,J/m^3$)
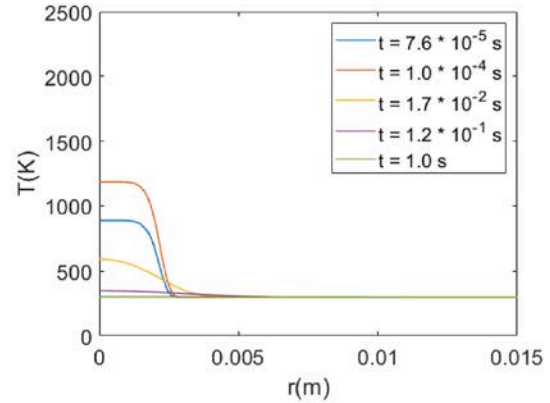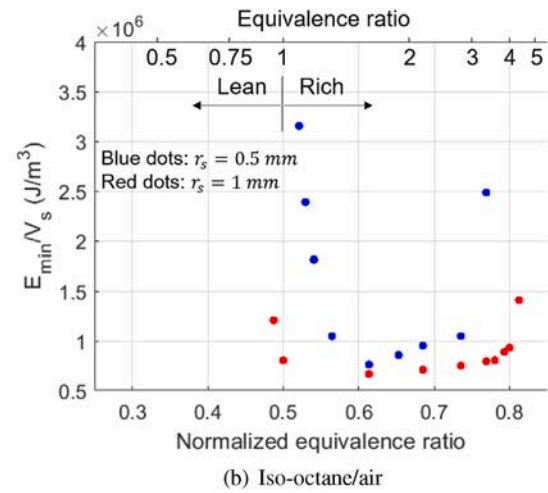
(b) The temperature history of an ignition failure. (iso-octane/air mixture, $\phi = 1.60$, spherical geometry, $r_s = 2\,mm$, $q = 5.10 \times 10^5\,J/m^3$)

Fig. 2. The temperature history of a successful ignition and an ignition failure.

(a) Methane/air

(b) Iso-octane/air

Fig. 3. Minimum ignition energy densities in dependence on the equivalence ratio with a spherical ignition source for two ignition radii ($r_s = 0.5$ mm and $r_s = 1$ mm) for methane/air and iso-octane/air mixtures. The small vertical line shows the location of $\varphi = 1$.

flame quenches after a while.

Within the flammability limits, the minimum ignition energy densities are comparable for both mixtures. This agrees with the results of Moorhouse et al. (1974). For both mixtures, with a relatively large spherical ignition source (r_s 1 mm), the minimum ignition energy density is almost constant within the flammability limits. It increases rapidly near the upper and lower flammability limits. This "U-shape" ignition energy density is also consistent with former studies (see e.g. Moorhouse et al. (1974)).

For both fuels, the ignition energy densities for smaller ignition radii r_s are higher than for large r_s. For smaller radii, we observe a notable dependence of MIE on the equivalence ratio also within the flammable range; compare the essentially "flat" curve described by the red points (r_s 1 mm) in Fig. 3 with the more variable dependence outlined by the blue points (r_s 0.5 mm).

For iso-octane/air mixtures, the MIE increases slightly with increasing equivalence ratio from φ_n 0.62 to φ_n 0.8 (φ 1.60 to φ 4), after that, the MIE increases faster when it approaches the upper flammability limit. On the other hand, at the lean side, the MIE starts to increase from φ_n 0.6 (φ 1.5). It is also observed that stoichiometric iso-octane/air mixtures with a small spherical ignition source cannot be ignited no matter how large the ignition energy is.

For lean mixtures with a small ignition source, the flame is strongly stretched, the stretch effect plays a very important role during the flame propagation. The spherical flame is positively stretched by the outward propagation, the heavy molecules will diffuse to the region with lower temperature, affecting the local equivalence ratio. Thus the flame is weakened and perhaps eventually quenches by the stretch effect (Law, 2006; Xin et al., 2012; Han and Chen, 2015). This phenomenon will be further discussed in section 3.2.

The dependence of minimum ignition energy densities on the equivalence ratio is shown in Fig. 4 for a cylindrical ignition source. The results are similar to the case of spherical ignition: the minimum ignition energy density is nearly independent of the equivalence ratio within the flammability limits and increases near the limits. The minimum ignition energy densities are higher for smaller ignition radius.

Some differences are observed, though. The increase of minimum ignition energy at the flammability limit is lower with cylindrical geometry than with the spherical geometry. The rapidly increasing minimum ignition energy for lean iso-octane/air mixture is less pronounced for the cylindrical geometry. This can be attributed to the different stretch rates for spherical and cylindrical flames.

For spherical and cylindrical geometries, the reaction zone is curved. Molecular transport at the reaction zone is then enhanced (relative to a planar front) by the curvature. Law (2006) uses the stretch rate by curvature to quantify this effect.
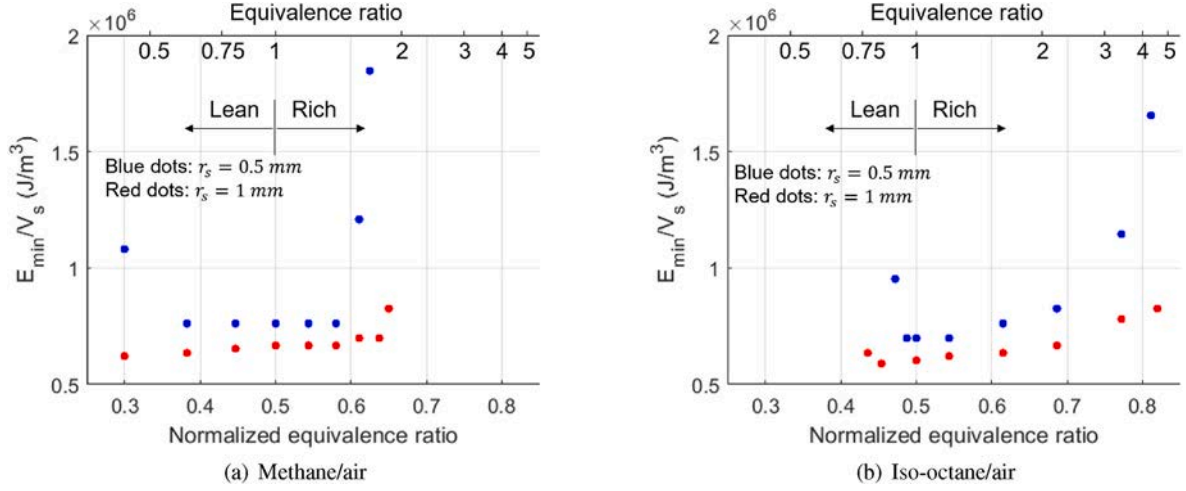
Fig. 4. Minimum ignition energy densities in dependence on the equivalence ratio with a cylindrical ignition source for two ignition radii ($r_s = 0.5$ mm and $r_s = 1$ mm) for methane/air and iso-octane/air mixtures. The small vertical line shows the location of $\varphi = 1$.

The stretch rate is defined as the ratio of the time derivative of the area of an infinitesimal element of the flame surface to the area itself. For outwardly propagating spherical flames (spherical flames that propagate in direction of larger radii), the stretch rate is

$$k = \frac{2}{R_f} \frac{dR_f}{dt} \tag{5}$$

and for outwardly propagating cylindrical flames, it is

$$k = \frac{1}{R_f} \frac{dR_f}{dt} \tag{6}$$

where R_f is the flame radius. This indicates a smaller stretch rate for cylindrical flames than for spherical flames at same flame radius, and thus a less pronounced influence of flame front curvature.
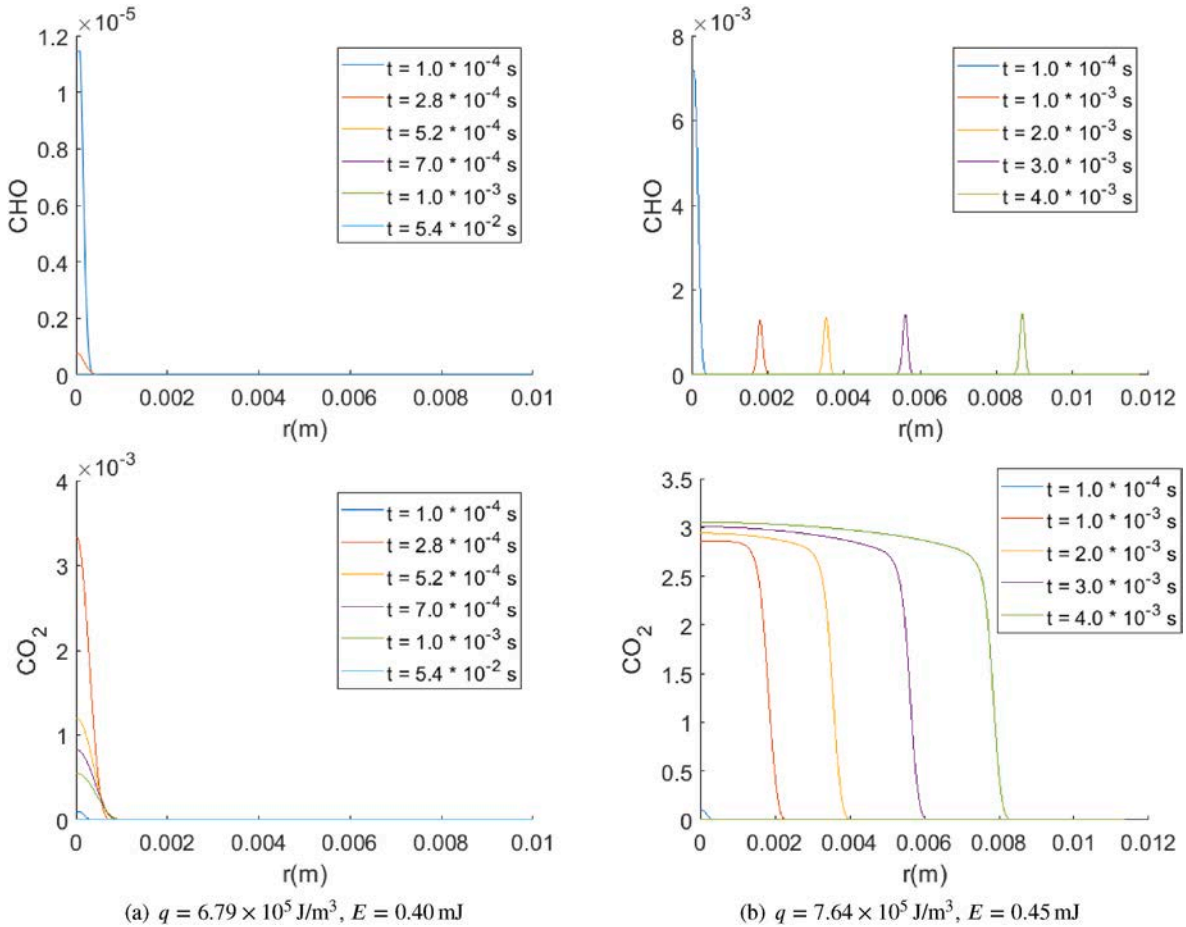

(a) $q = 6.79 \times 10^5$ J/m³, $E = 0.40$ mJ

(b) $q = 7.64 \times 10^5$ J/m³, $E = 0.45$ mJ

Fig. 5. CHO and CO_2 profiles for stoichiometric methane/air mixture with spherical ignition source ($r_s = 0.5$ mm), with no successful ignition (left) and successful ignition (right). Note the different scales on the y-axis for both CO_2 and CHO on the left vs. right side.

In order to find out the reason for the differences between the two fuels, we first calculated minimum ignition energies for mixtures with equal diffusivity ($Le = 1$). The results show that the difference of minimum ignition energies with same ignition radius are much smaller compared to the results using detailed calculations. For example, for detailed calculations, when the ignition radius is 1 mm, the MIE of stoichiometric iso-octane/air mixture is about 1.2 times that of a stoichiometric methane/air mixture. However, if all Lewis numbers are set to 1, the MIE of stoichiometric iso-octane/air mixture is only 2% larger than that of a stoichiometric methane/air mixture. The difference between spherical and cylindrical geometries also suggests that the curvature effect due to the large Lewis number of lean to stoichiometric iso-octane/air mixtures might be the reason that the two fuels have different MIEs with same ignition source size. In the next section, this curvature effect on the flame development is further discussed.

3.2. The effect of curvature on minimum ignition energy

As mentioned in the last section, there is a rapid increase of minimum ignition energy density for iso-octane/air mixtures from $\varphi = 1.5$ ($\varphi_n = 0.6$) to lean mixtures with spherical geometry. The reason is that, if the ignition source is small, after the flame kernel is formed in the ignition volume, the flame radius is also small and the flame curvature is large, hence the flame is strongly stretched after the ignition, flame extinction might occur.

To further understand how the curvature affects the minimum ignition energy, the profiles of CO_2 and CHO are investigated. The values of CHO and CO_2 in Fig. 5 are given as specific mole numbers, i.e., as the ratio of mass fraction w_i and molar mass M_i of the species:

$$Y_i = \frac{w_i}{M_i}, \quad i = CHO, CO_2. \tag{7}$$

The profiles of CO_2 are used to assess to which extent the gas mixture in the ignition volume is already burned; CO_2 is thus used as a kind of reaction progress indicator. The temperature, which is used in section 3.1 as an indicator of flame propagation and flame extinction, is not suitable here, because it is hard to tell the difference between no flame kernel formation and flame extinction using the temperature profiles. The profiles of CHO are used as representative for the heat release rate. Large values of CHO indicate regions of large chemical reaction rates, thereby outlining the approximate position of the flame front (Paul and Najm, 1998; Najm et al., 1998).

For the methane/air mixture shown in Fig. 5, it is clearly seen that with an ignition energy density slightly below the minimum ignition energy, only a small amount of CO_2 is formed, which means that the energy is not enough to ignite the mixture in the ignition volume. However, above the minimum ignition energy, we can see the formation of CO_2 and the propagation of the flame.

Here the ignition source is only 0.5 mm, but we can still see that for stoichiometric methane/air mixture, the large curvature will not cause the flame to quench; Whenever the ignition energy is large enough to ignite the mixture in the ignition volume, a self-sustained flame will be formed. The reason is that, for methane/air mixtures, whose Lewis number is approximately equal to 1, the flame speed is nearly unaffected by the curvature effect (Law, 2006). As a result, for methane/air mixtures, the minimum ignition energy is also nearly unaffected by the curvature effect.

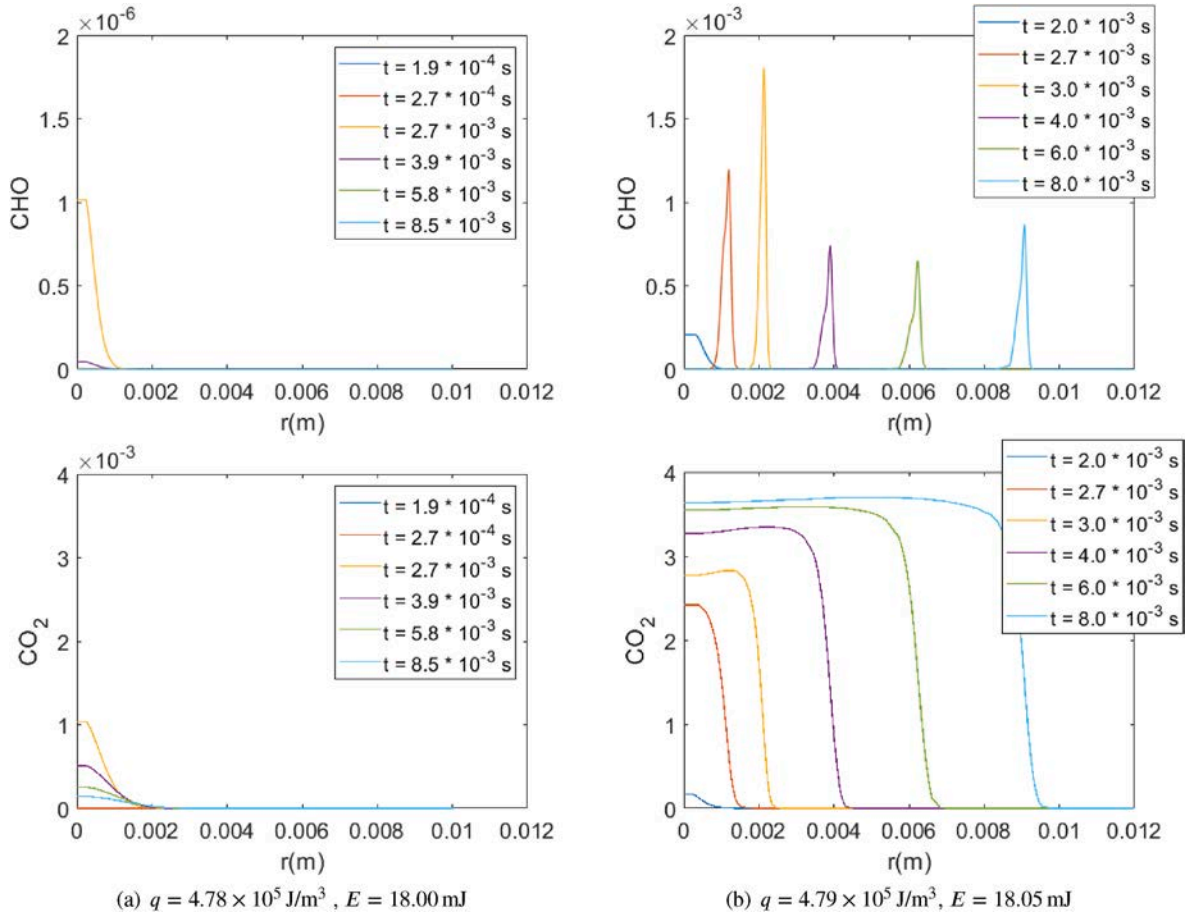On the other hand, the stoichiometric iso-octane/air mixture

(a) $q = 4.78 \times 10^5$ J/m^3, $E = 18.00$ mJ

(b) $q = 4.79 \times 10^5$ J/m^3, $E = 18.05$ mJ

Fig. 6. CHO and CO_2 profiles for stoichiometric iso-octane/air mixture with spherical ignition source ($r_s = 2$ mm), with no successful ignition (left) and successful ignition (right). Note the different scales on the y-axis for both CO_2 and CHO on the left vs. right side.

behaves differently. When the ignition source is relatively large (r_s 2 mm), the curvature effect will not cause flame extinction. As is shown in Fig. 6, above the minimum ignition energy, the formation of CO_2 and the propagation of the flame can be observed; with an ignition energy lower than the minimum ignition energy, the formation of CO_2 is very limited, which implies that no flame kernel is formed at all.

However, when the ignition source is smaller (r_s 1 mm), as is shown in Fig. 7, flame extinction caused by the curvature effect is clearly observed. Here the minimum ignition energy density is 7.11×10^5 J/m^3. In contrast to the results of r_s 2 mm, where no ignition was found below the minimum ignition energy, here, even when the source energy density is 6.90×10^5 J/m^3 (below the MIE), the mixture in the ignition volume is still ignited. During the first 2 ms, the CO_2 formation and the propagation of the peak of CHO are very similar to the case of normal flame propagation. But when the reaction front (as identified by the peak of CHO) has moved about 2 mm away from the ignition source, the flame quenches. The ignition energy density q 6.90×10^5 J/m^3 is therefore enough to generate a flame kernel, but the flame cannot propagate further and extinguishes. We define the distance between the CHO peak and the left boundary of the calculation domain (r 0) as the flame radius. The evolution of this for the different cases is shown in Fig. 8.

For r_s 2 mm, if the ignition energy is below the minimum ignition energy (q 4.78×10^5 J/m^3, blue curves in Fig. 8(a)), no flame kernel formation is observed. The flame radius defined by the distance between the CHO peak and the left boundary of the calculation domain (r 0) stays at 0, while the maximal temperature rises up to about 1200 K because of the external source, and then decreases back to 298 K.

However, when the ignition energy is slightly higher than the minimum ignition energy (q 4.79×10^5 J/m^3, red curves in Fig. 8(a)), a self-sustained flame is observed. After about 0.0025 s, there's a sudden increase of the flame radius, and the maximal temperature also increases rapidly to about 2300 K, then the flame propagation is observed. If the ignition energy is even higher than q 4.79×10^5 J/m^3 (q 4.89×10^5 J/m^3, yellow curves in Fig. 8(a)), the flame radius and the flame temperature rise even earlier.

For r_s 1 mm, if the ignition energy is slightly higher than the minimum ignition energy (q 7.11×10^5 J/m^3, yellow curves in Fig. 8 (b)), flame propagation is observed. After the formation of the flame kernel, the flame propagation is supported by the excess enthalpy from the external ignition energy, the flame propagation speed decreases because of the curvature effect; then, after the flame reaches a certain radius (about r 2.5 mm), a transition phase occurs and the flame propagation speed increases until it propagates as a self-sustained flame (Kim et al., 2013; Wang et al., 2019; Kelley and Law, 2009). On the other hand, if the ignition energy density q is a little bit smaller than the minimum ignition energy (q 6.90×10^5 J/m^3, red curves in Fig. 8(b)), the flame will propagate to a radius about 2.2 mm, which is smaller than the critical radius, and then quenches. If the ignition energy density q is even smaller than 6.90×10^5 J/m^3 (q 6.15×10^5 J/m^3, blue curves in Fig. 8(b)), the flame quenches at even smaller radii.

However, for r_s 0.5 mm, no flame propagation can be observed, no matter how large the ignition energy is. For example, when the ignition energy is 4.24×10^6 J/m^3, the flame kernel formation is observed, the flame propagates to about r 1.5 mm and then quenches. When the ignition energy is smaller, the flame quenches at a smaller radius.
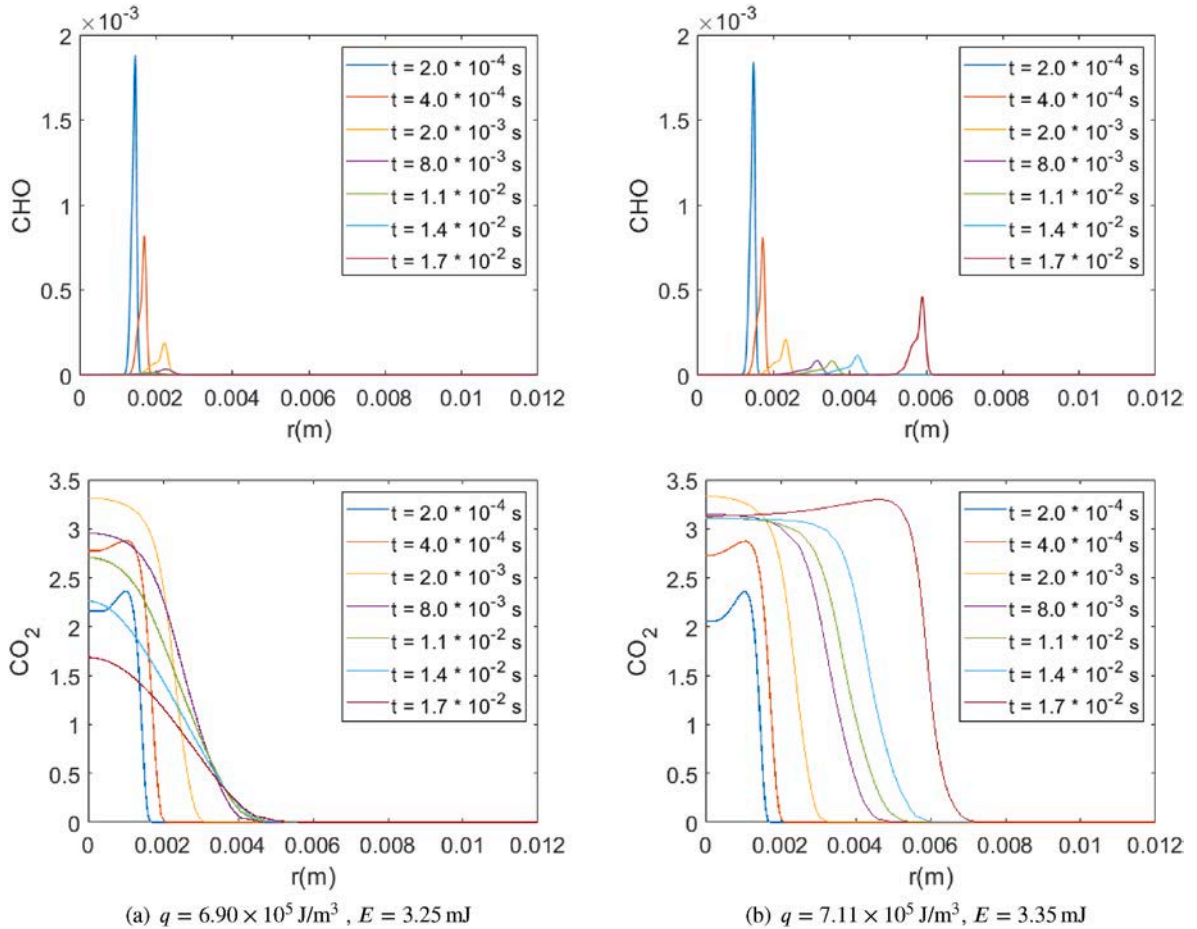

(a) $q = 6.90 \times 10^5$ J/m^3, $E = 3.25$ mJ

(b) $q = 7.11 \times 10^5$ J/m^3, $E = 3.35$ mJ

Fig. 7. CHO and CO_2 profiles for stoichiometric iso-octane/air mixture with spherical ignition source ($r_s = 1$ mm), with flame extinction (left) and flame propagation (right).
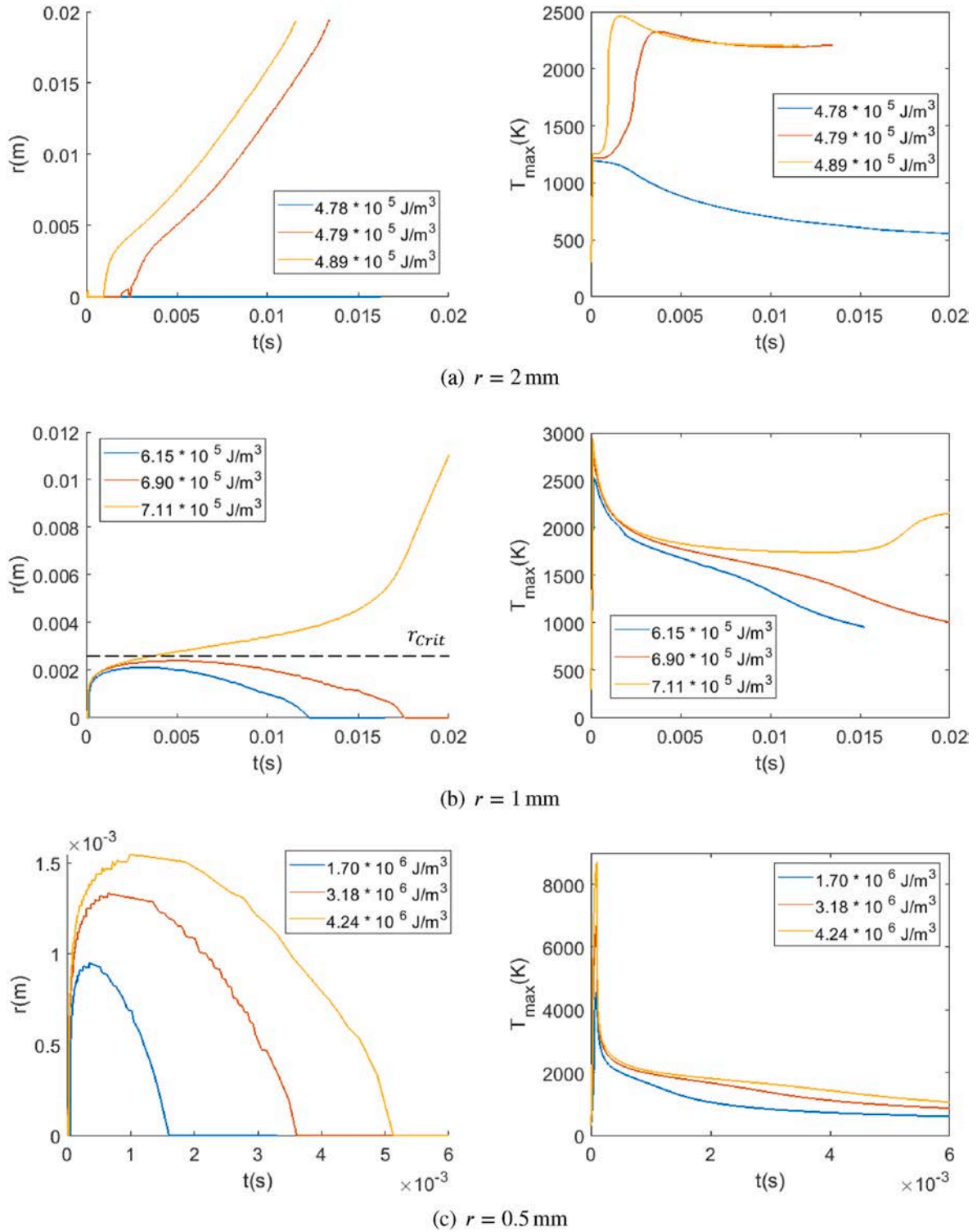
Fig. 8. Temporal development of the flame radius and of the maximal temperature for stoichiometric iso-octane/air mixtures with a spherical source $r_s = 2$ mm (top) $r_s = 1$ mm (middle) and $r_s = 0.5$ mm (bottom).

The amount of CHO formed during the ignition duration and ignition delay time is very limited, when the mixture in the ignition volume is not yet ignited. It is observed, that the flame radius starts at 0 mm at first, and shows a sudden increase after the ignition delay time. In Fig. 8(a), the sudden increase of the flame radius after the ignition delay time is clearly to be seen. In Fig. 8(b) and (c), the ignition energies are very large, the temperature in the middle of the heated gas after the ignition duration are also very high, the ignition delay times are so small

compared to the entire calculation duration, that they can't be observed in the figures.

According to He (2000), Kelley et al. (2009), Ko et al. (1991), and Chen et al. (2011), a critical flame radius exists for a positively stretched spherical flame with $Le > 1$. If the flame can reach this critical radius, it will evolve into a propagating flame. Otherwise, the flame quenches. The Lewis number of iso-octane/air mixtures increases when the equivalence ratio decreases (Lawes et al., 2012), the critical radius for

the lean mixtures is higher, more energy is needed to reach the critical radius. This critical flame radius is indicated by the horizontal dashed line in Fig. 8(b). For stoichiometric iso-octane/air mixtures, the critical flame radius is about r 2.5 mm.

For the ignition source radius r_s 2 mm, after the ignition delay time, because of the thermal expansion, the flame radius already increases up to the critical radius of stoichiometric iso-octane/air flame (about 2.5 mm). The curvature effect is less pronounced, which means that if a flame kernel is formed, the flame can propagate.

This can also explain why the stoichiometric iso-octane/air mixture cannot be ignited with a spherical source r_s 0.5 mm. As it is shown in Fig. 8(c), the temperature in the center increases up to 8000 K, and the initiated flame still cannot reach the critical flame radius for stoichiometric iso-octane/air mixture. As a result, the flame quenches and the rest of the mixture remains unignited.

3.3. The dependence of minimum ignition energies on the ignition radius for iso-octane/air mixtures

As discussed in section 3.2, for mixtures like stoichiometric iso-octane/air with $Le > 1$, the flame kernel must reach a certain radius for a successful flame propagation (He and Law, 1999; Kelley et al., 2009). This indicates that there exist two kinds of minimum ignition energies: (1) MIE for a successful ignition in the ignition volume, and (2) MIE for a successful flame propagation.

Fig. 9 shows the dependence of minimum ignition energy densities on the ignition radius for stoichiometric iso-octane/air mixtures with spherical ignition sources. Results show that if $r_s > 1.5$ mm, the minimum ignition energy densities for the flame initiation in the ignition volume and for a successful flame propagation are the same. Also, the minimum ignition energy density decreases slightly with increasing ignition radius due to heat conduction becoming less important. This means that either the mixture can be ignited and the flame can propagate, or the energy is not enough to ignite the mixture at all. The reason is that, for stoichiometric iso-octane/air mixtures, if $r_s > 1.5$ mm, the flame can almost reach the critical radius after the ignition because of the thermal expansion, so the curvature effect will not cause flame extinction. However, as $r_s < 1.5$ mm, a third region becomes more significant, where the energy is enough to ignite the mixture ignition kernel, but not enough for the flame to propagate to the critical radius, the flame quenches because of the curvature effect.
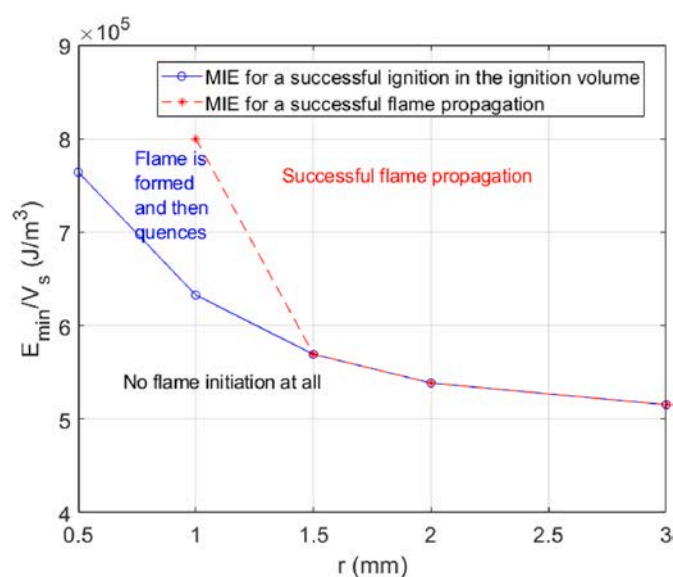
4. Conclusion

In this study, the dependence of the minimum ignition energy (MIEs) on the fuel composition, the ignition source geometry and the ignition source size is investigated for methane/air and iso-octane/air mixtures using one-dimensional simulations. Although some phenomena like the influence of a non-symmetric flow field are unable to be calculated by one-dimensional simulations, minimum ignition energies for premixed mixtures allow important insight into the underlying processes.

The MIE vs. equivalence ratio diagrams for both fuels shows the familiar "U"-shaped curves. Within the flammability limits, the MIE stays almost constant, and it increases rapidly at the limits. The MIEs for both fuels are also similar within the flammability limits.

The Lewis number for methane/air mixtures is close to 1, the curvature effect on the minimum ignition energy is negligible, even with small ignition radii, flame curvature will not cause flame extinction. However, for iso-octane/air mixture with $\varphi < 1.5$, where the Lewis number is above 1 and further increases when the mixture gets leaner, the flame curvature strongly affects the flame propagation. If the ignition source is small, even if the ignition energy is large enough for the formation of a flame kernel, the flame might still quench because of the strong stretch. This phenomenon is less pronounced for a cylindrical ignition kernel, because the stretch rate for a cylindrical flame is smaller and thus the curvature effect is smaller compared to the spherical case.

Furthermore, we investigated the flame propagation for spherical iso-octane/air flames. Results show that for larger ignition sources, the mixture can either be ignited in the center and the flame is able to propagate, or the mixture cannot be ignited at all. On the other hand, with a smaller ignition source, it is possible that a flame is first formed, but then quenches.

For $r_s > 1.5$ mm, the minimum ignition energy densities for a flame initiation in the ignition volume and for a successful flame propagation are the same. But for $r_s < 1.5$ mm, there's a difference between the two minimum ignition energy densities. The difference becomes larger for smaller ignition radii.

Fig. 9. The dependence of minimum ignition energy on ignition radius for stoichiometric iso-octane/air mixture with spherical ignition source.

References

Abdel-Gayed, R.G., Bradley, D., Hamid, M.N., Lawes, M., 1985. Lewis number effects on turbulent burning velocity. In: Symp. (Int.) Combust., vol. 20, pp. 505–512. https://doi.org/10.1016/S0082-0784(85)80539-7.

Andrae, J.C.G., Brinck, T., Kalghatgi, G.T., 2008. HCCI experiments with toluene reference fuels modeled by a semidetailed chemical kinetic model. Combust. Flame 155, 696–712. https://doi.org/10.1016/j. combustflame.2008.05.010.

Chakrabarty, A., Mannan, S., Cagin, T., 2016. Process safety. In: Chakrabarty, A., Mannan, S., Cagin, T. (Eds.), Multiscale Modeling for Process Safety Applications. Butterworth-Heinemann, Boston, pp. 5–110.

Chen, Z., Burke, M.P., Ju, Y., 2011. On the critical flame radius and minimum ignition energy for spherical flame initiation. Proc. Combust. Inst. 33, 1219–1226. https://doi.org/10.1016/j.proci.2010.05.005.

Clarke, A., 2002. Calculation and consideration of the lewis number for explosion studies. Process Saf. Environ. Protect. 80, 135–140. https://doi.org/10.1205/095758202317576238.

Dahn, C.J., Dastidar, A.G., 2003. Requirements for a minimum ignition energy standard. Process Saf. Prog. 22, 43–47. https://doi.org/10.1002/prs. 680220106.

Frendi, A., Sibulkin, M., 1990. Dependence of minimum ignition energy on ignition parameters. Combust. Sci. Technol. 73, 395–413. https://doi.org/10.1080/00102209008951659.

Han, W., Chen, Z., 2015. Effects of soret diffusion on spherical flame initiation and propagation. Int. J. Heat Mass Tran. 82, 309–315. https://doi.org/10.1016/j.ijheatmasstransfer.2014.11.062.

Hansen, O.R., Middha, P., 2008. Cfd-based risk assessment for hydrogen applications. Process Saf. Prog. 27, 29–34. https://doi.org/10.1002/prs. 10213.

He, L., 2000. Critical conditions for spherical flame initiation in mixtures with high lewis numbers. Combust. Theor. Model. 4, 159–172. https://doi.org/10.1088/1364-7830/4/2/305.

He, L., Law, C.K., 1999. On the Dynamics of Transition from Propagating Flame to Stationary Flame Ball. https://doi.org/10.2514/6.1999-325.

Kelley, A.P., Jomaas, G., Law, C.K., 2009. Critical radius for sustained propagation of spark-ignited spherical flames. Combust. Flame 156, 1006–1013. https://doi.org/10.1016/j.combustflame.2008.12.005.

Kelley, A.P., Law, C.K., 2009. Nonlinear effects in the extraction of laminar flame speeds from expanding spherical flames. Combust. Flame 156, 1844–1851. https://doi.org/10.1016/j.combustflame.2009.04.004.

Kim, H.H., Won, S.H., Santner, J., Chen, Z., Ju, Y., 2013. Measurements of the critical initiation radius and unsteady propagation of n-decane/air premixed flames. Proc. Combust. Inst. 34, 929–936. https://doi.org/10.1016/j. proci.2012.07.035.

Ko, Y., Anderson, R.W., Arpaci, V.S., 1991. Spark ignition of propane-air mixtures near the minimum ignition energy: Part I. An experimental study. Combust. Flame 83, 75–87. https://doi.org/10.1016/0010-2180(91) 90204-O.

Law, C.K., 2006. Combustion Physics. Cambridge University Press.

Lawes, M., Ormsby, M.P., Sheppard, C.G.W., Woolley, R., 2012. The turbulent burning velocity of iso-octane/air mixtures. Combust. Flame 159, 1949–1959. https://doi.org/10.1016/j.combustflame.2011.12.023.

Lewis, B., von Elbe, G., 1987. The reaction between hydrocarbons and oxygen. In: Lewis, B., von Elbe, G. (Eds.), Combustion, Flames and Explosions of Gases, third ed. Academic Press, San Diego, pp. 96–211.

Maas, U., Warnatz, J., 1988. Ignition processes in hydrogen/oxygen mixtures. Combust. Flame 74, 53–69. https://doi.org/10.1016/0010-2180(88) 90086-7.

Moorhouse, J., Williams, A., Maddison, T.E., 1974. An investigation of the minimum ignition energies of some C1 to C7 hydrocarbons. Combust. Flame 23, 203–213. https://doi.org/10.1016/0010-2180(74)90058-3.

Najm, H.N., Paul, P.H., Mueller, C.J., Wyckoff, P.S., 1998. On the adequacy of certain experimental observables as measurements of flame burning rate. Combust. Flame 113, 312–332. https://doi.org/10.1016/S0010-2180(97) 00209-5.

Paul, P.H., Najm, H.N., 1998. Planar laser-induced fluorescence imaging of flame heat release rate. Symp. (Int.) Combust. 27, 43–50. https://doi.org/10.1016/S0082-0784 (98)80388-3.

Renner, T., 2007. Quantities, Units and Symbols in Physical Chemistry. The Royal Society of Chemistry.

Smith, G.P., Golden, D.M., Frenklach, M., Moriarty, N.W., Eiteneer, B., Goldenberg, M., Bowman, C.T., Hanson, R.K., Song, S., Jr, W.C.G., Lissianski, V.V., Qin, Z., . Gri 3.0 http://www.me.berkeley.edu/gri_mech.

Takashi, H., Kimitoshi, T., 2006. Laminar Flame Speeds of Ethanol, N-Heptane, Iso-Octane Air Mixtures.

Wang, Y., Han, W., Chen, Z., 2019. Effects of fuel stratification on ignition kernel development and minimum ignition energy of n-decane/air mixtures. In: Proc. Combust. Inst., vol. 37, pp. 1623–1630. https://doi.org/10.1016/j.proci. 2018.05.087.

Warnatz, J., Maas, U., Dibble, R., 2006. Combustion: Physical and Chemical Fundamentals, Modeling and Simulation, Experiments, Pollutant Formation. Springer, Berlin, Heidelberg.

Xin, Y., Sung, C.J., Law, C.K., 2012. A mechanistic evaluation of soret diffusion in heptane/air flames. Combust. Flame 159, 2345–2351. https://doi.org/10.1016/j.combustflame.2012.03.005.